

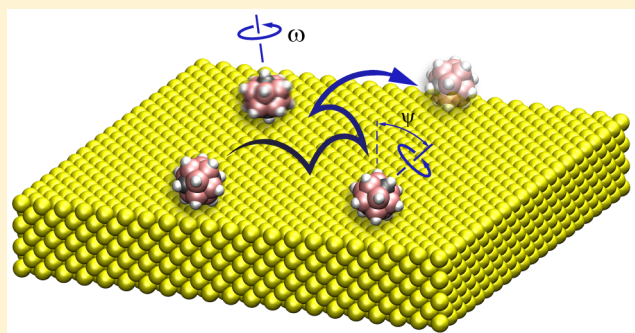
Mechanism of 1,12-Dicarba-closo-dodecaborane Mobility on Gold Substrate as a Nanocar Wheel

Seyed Mohammad Hosseini Lavasani,* Hossein Nejat Pishkenari,* and Ali Meghdari*

Nano Robotics Laboratory, Center of Excellence in Design, Robotics and Automation (CEDRA), Mechanical Engineering Department, Sharif University of Technology, Tehran, Iran

Supporting Information

ABSTRACT: We studied the mobility of *p*-carborane on a gold surface by analyzing the potential energy surfaces (PES) and simulating the motion of *p*-carborane using the classical molecular dynamics (MD) method. In the first section, we calculated the PES of *p*-carborane molecules on a gold surface during pure translation (sliding) and pure rotation independently and then employed this PES to predict the probable motion of *p*-carborane. These calculations were performed in several major orientations during sliding as well as different fixed positions during rotational movements to enable us to find the *p*-carborane motion threshold on a gold surface. In the second section, we use classical MD in isothermal conditions to specify the regime of motion of *p*-carborane at different temperatures. We found that by raising the temperature, three different regimes of motion may be observed: jumps to adjacent cells, long jumps, and continuous motion. To better understand the change of motion regime of *p*-carborane on the gold surface, we proposed a quantified parameter for describing the motion. Both MD and PES results demonstrated that rotation around a horizontal axis is more difficult than pure sliding, while rotation around a vertical axis is easier and likely to occur even at low temperatures. The results of this study not only provide quantitative criteria for specifying the regime of motion of *p*-carborane on a gold surface but also can be used to estimate the behavior of thermally driven or motorized *p*-carborane-based nanocars and their motion on similar substrates.



1. INTRODUCTION

In recent years, fabrication of molecular-scale mechanical and electronic devices has been the subject of vigorous study. Molecular-scale machines such as elevators, switches, and robots are some examples of this trend.¹ Molecular machines enable us to transport materials, medication, and energy at the nanoscale. Molecular machines were first proposed by Nobel Prize winner Richard Feynman in 1960,² and the first molecular machine was fabricated in the early 1980s using photoisomerization of azobenzene molecules.³ Different approaches are used to fabricate molecular machines. In the bottom-up approach, molecular components are assembled to create microscopic structures.⁴ The advantage of this approach is that it can use the self-assembly ability of small molecules to create complex and powerful nanomachines that can handle large numbers of payloads or atoms simultaneously, whereas other approaches (e.g., photolithography and related techniques) are nearing their fabrication limits.

In recent years, James Tour's research group has proposed several molecular machines.^{5–7} These molecules are called nanocars because of their appearance which is composed of a "chassis" and a number of "wheels". The proposed nanocar designs include nanocars with C₆₀, *p*-carborane,^{6,8–10} ruthenium-based,¹¹ and recently adamantane¹² wheels. Some proposed designs have the ability to transport a payload¹³ or

self-assemble.^{14,15} The motion of these nanocars is the result of temperature-induced vibrations of the substrate atoms. As a result, the motion is random and nonunidirectional. Because controlling the direction of motion is often desired, nanocars are designed to enhance or inhibit motion in a specific direction. The nanocooper and nanocaterpillar were designed to reduce the motion in a lateral direction, making the translation mainly parallel to the chassis axle. The same approach was used to design angled nanocars for improving circular motion and trimer nanocars for rotating around its pivot.⁴ For better control over their motion, motorized nanocars have been designed.^{16–18} The nanoworm has an azobenzene molecular motor in its chassis which is activated by light.¹⁹ When a particular wavelength of light is absorbed by the azobenzene molecule, trans–cis or cis–trans photoisomerization occurs. As a result, the chassis shows a worm-like movement.

Nanocars have the potential to be used as minutely controlled molecular transportation methods. The first step toward understanding the abilities of nanocars is studying their motion on different substrates. The mobility of the first C₆₀–

Received: March 1, 2016

Revised: May 19, 2016

based nanocar was studied using scanning tunneling microscopy (STM) shortly after its fabrication.⁵ It was observed that its motion is more probable in the longitudinal direction than the lateral direction and rotations may occasionally occur. In a separate study, the motion of a *p*-carborane-based nanocar on nonmetallic surfaces was studied using the fluorescent marker tracking method, and the diffusion coefficient was measured.^{20,21} Because of the limitations of the STM technique, only conductive surfaces can be imaged and the frequency of imaging is limited depending on the imaging area.⁵ A gold substrate is often used for imaging purposes because of its conductivity and stability. The advantage of the fluorescent tracking method is that it induces less perturbation in the system than the STM technique because it is not in direct contact with the system. However, a fluorescent marker must be attached to the chassis which changes the dynamic properties of the system. Also because the resolution achieved with this method is less than that of the STM techniques, some details cannot be captured. Because studying the dynamics of the wheels requires subnanosecond resolution, neither of these methods is suitable for our purposes.

Although few ab initio and classical MD studies have been performed on nanocars, C_{60} -based nanocars and their parts^{22–24} have been mostly studied on a gold surface using these methods. Akimov et al. studied the motion of a rigid nanocar,²⁵ and Konyukhov et al. studied a flexible nanocar with a Z-shaped chassis on a gold surface.²⁶ A flexible C_{60} -based nanocar in the presence of a STM instrument has been simulated by Akimov et al.²⁷ While the components of a nanocar, e.g. wheels, have been studied, the motion of *p*-carborane-based nanocars on metallic or nonmetallic surfaces²⁸ has not been widely studied. Therefore, experimental data are available for carborane adsorption on different surfaces, and in some studies ab initio methods have even been used. These studies include STM technique, photoemission, electron spectroscopy, and density functional theory (DFT) calculations for studying chemisorption and physisorption of carborane on different surfaces including Pt(111),²⁹ Cu(100),³⁰ Co(111), Au(111),^{31–33} and hydrated silica.³⁴ In one study was observed that ortho-carborane on Cu(100) experiences molecular adsorption below 180 K and dissociative adsorption above 300 K. However, molecularly adsorbed *o*-carborane is stable at 300 K. Also, the desorption rate of molecularly adsorbed *o*-carborane has two maxima at 450 and 600 K. At 450 K, *o*-carborane desorbs molecularly but at 600 K it is desorbed dissociatively.³⁰ *o*-Carborane is also stable on Pt(111) for temperatures below 400 K.²⁹ In another study, ab initio calculation states that the binding energy between *p*-carborane and hydrated silica is 8 kJ/mol using the DFT method, and experimental data validated this calculation. It was found that hydrogen bonding is the dominant molecular interaction in this case.³⁴

Because *p*-carborane is used as a wheel in many nanocars, investigating the mobility of this molecule is necessary to understand the motion of these nanocars. As mentioned above, several studies have focused on the adsorption of carborane isomers on transition metals and nonmetals, but limited information is available on the motion of this molecule on gold. In this paper, we study the motion of carborane using two different approaches. We first study *p*-carborane motion by calculating its potential energy surfaces (PES) and their variation during pure transitional or pure rotational motion on a gold substrate. In this method, the potential energy is

calculated at different positions on the substrate and in different orientations. Potential energy is used to predict potential movements in each condition. We then study the motion of *p*-carborane on the gold substrate using classical molecular dynamics (MD).

This paper is organized as follows. In section 2, the model setup and simulation parameter for the aforementioned approaches are explained in detail. In section 3, first the results of both approaches are presented and discussed. Then the results are compared and analyzed together to understand the motion of *p*-carborane molecules on gold substrates. In the final section, our main conclusions are presented.

2. MODELS AND SIMULATION DETAILS

In this section, detailed modeling procedures for analyzing the variation of PES and classical MD approaches are explained.

2.1. Potential Energy Approach. To calculate the PES of *p*-carborane on a gold substrate, we first need to find the equilibrium state of *p*-carborane molecules (see Figure 1). First-

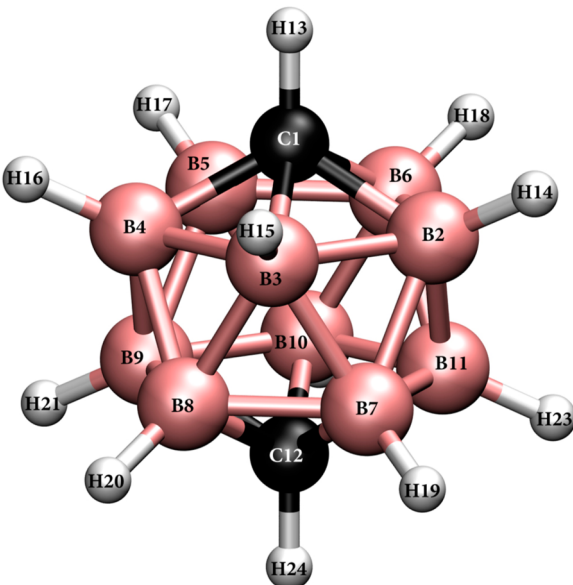


Figure 1. Equilibrium structure of 1,12-vertex carborane molecules obtained using B3LYP/6-31++G(d,p) calculation.

principles DFT calculations were performed using the Becke, three-parameter, and Lee-Yang-Parr (B3LYP) exchange-correlation functional to achieve an optimized structure and the total energy of the *p*-carborane molecule. Calculations were performed using a 6-31++G(d,p) basis set employing the NWChem 6.5 package.³⁵ The *p*-carborane structure was optimized in gaseous form, and the absolute energy was calculated as -332.1538 hartree. Some of the calculated bond lengths are presented in Table 1. The minimization was verified by studies which used ab initio methods to find the equilibrium structure, vibrational properties,^{36,37} and experimental bond length³⁸ of *p*-carborane molecules.

A gold substrate Au(001) with a face-centered cubic (FCC) lattice structure crystal was used for calculating PES. The substrate dimensions were $20a \times 20a$ in the $x-y$ plane and $3a$ height in the z -direction, and the FCC crystalline direction was chosen parallel to the z -axis, where a is the lattice constant of the gold crystal and equals 4.078 Å at 300 K.³⁹ The lattice constant of gold varies slightly with temperature.^{40,41} To ensure

Table 1. Equilibrium Bond Length and Absolute Energy of *p*-Carborane in Comparison with Different Levels of Theory and Experiment

atom type	unit	B3LYP/6-31++G(d,p)	HF/6-31G** ^a	B3LYP/cc-pVDZ ^b	HF/cc-pVDZ ^b	experiment ^c
C1–B2	Å	1.708	1.708	1.711	1.712	1.710 ± 0.011
B2–B3	Å	1.786	1.793	1.774	1.779	1.792 ± 0.007
B2–B7	Å	1.767	1.772	1.791	1.798	1.772 ± 0.013
C–H	Å	1.084	—	1.089	1.079	1.150 ± 0.090
B–H	Å	1.182	—	1.191	1.185	1.216 ± 0.021
absolute energy	Hartree	−332.1538	−329.6669	−332.1249	−329.6641	—

^aHF/6-31G** data taken from ref 36. ^bB3LYP/cc-pVDZ and HF/cc-pVDZ data taken from ref 37. ^cExperimental data taken from ref 38.

that using the value of the lattice constant at 300 K does not invalidate the results at higher or lower temperatures, the PES of *p*-carborane on a gold surface was calculated based on the temperature-adjusted lattice constant values. It was found that the results from constant and temperature-adjusted values differed by less than 1%. As a result, the value was assumed to be constant for all further PES calculations.

Both the gold substrate and the *p*-carborane molecule were assumed to be internally rigid in the PES approach. In this situation, the intramolecular potential energy of *p*-carborane and the internal interactions of the gold atoms remain constant, and only the change in nonbond interactions between the *p*-carborane and the gold substrate are considerable. The potential between *p*-carborane and gold was calculated using a 6–12, Lennard-Jones (LJ) potential as follows:

$$E_{ij}^{\text{LJ}} = 4\epsilon_{ij} \left[-\left(\frac{\sigma_{ij}}{r_{ij}} \right)^6 + \left(\frac{\sigma_{ij}}{r_{ij}} \right)^{12} \right] \quad (1)$$

where ϵ_{ij} represents the equilibrium nonbond energy; σ_{ij} is the distance at which the interaction potential is zero, and r_{ij} is the distance between two atoms of type of i and j . In the following, we refer to two studies to estimate nonbond interactions between *p*-carborane and gold. In ref 42, Heinz et al. proposed LJ parameters for several FCC metals and interface properties with water and bio-organic molecules. Another study used classical MD simulation in isobaric conditions and different temperatures to present LJ parameters for intermolecular interaction between carboranes.⁴³ In our system, which consists of several atomic types, Lorentz–Berthelot mixing rules (eq 2) were used to calculate the gold–carborane intermolecular potential.^{44,45} It is obvious that the mixing rules between any atom types are approximate, but the simulation test revealed that from the available LJ parameters for the gold, this parameter⁴² is more current and performs well in tests. Table 2 shows the LJ parameters used in this paper. In addition, the cutoff radius of 15 Å ($r_{\text{cutoff}} > 4.3\sigma_{\text{max}}$) is used.

$$\epsilon_{ij} = \sqrt{\epsilon_i \epsilon_j}, \quad \sigma_{ij} = \frac{\sigma_i + \sigma_j}{2} \quad (2)$$

2.2. Molecular Dynamics Approach. We have simulated the motion of *p*-carborane at different temperatures to evaluate the effect of temperature on the regime of motion. Classical MD simulations were performed with the Large-scale Atomic/Molecular Massively Parallel Simulator (LAMMPS) package⁴⁶ in isothermal conditions, and the velocity Verlet method was used for integration over time. A visual molecular dynamics (VMD) program was employed for visualization and graphics.⁴⁷ At the beginning of the simulation, the *p*-carborane molecule

Table 2. Parameters Set for 6–12, LJ Potential to Simulate the Carborane–Gold Nonbond Interaction

atom type	ϵ (meV)	σ (Å)
Au–Au ^a	229.4	2.63
C–C ^b	4.104	3.45
B–B ^b	1.847	4.31
H–H ^b	0.4249	2.97

^aAu–Au data taken from ref 42. ^bC–C, B–B, and H–H data taken from ref 43.

was placed in the middle of the substrate and at the equilibrium distance from the surface (see Figure 2). All the MD

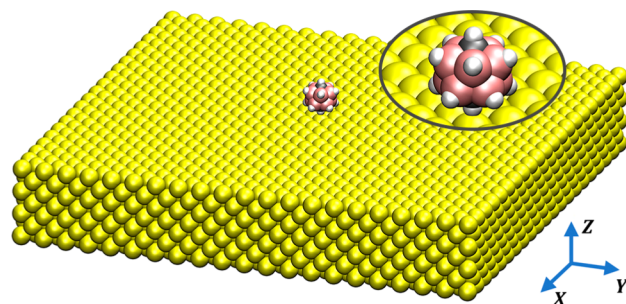


Figure 2. *p*-Carborane on a gold substrate. In x and y -directions, periodic boundary condition was used.

simulations were performed for 8 ns with the integration time step set to 1 fs to achieve sufficient accuracy. First, the potential energy of the entire system was minimized; then, the system was relaxed for 100 ps. A canonical ensemble (NVT) in which the temperature was controlled with a Nosé–Hoover thermostat was used.^{48,49} The thermostat was applied to the substrate and the *p*-carborane molecule independently, and the velocity of the *p*-carborane center-of-mass was ignored in the thermostat calculations. In our calculations, the thermal inertia parameter value is set to 100 timesteps. The system was simulated at different temperatures ranging from 5 to 500 K. A Au(001) substrate was used for MD simulations with dimensions the same as those previously reported in the PES approach. Although the lattice constant varies slightly with temperature,^{40,41} an accurate lattice constant value for each temperature was used to avoid temperature-induced stress in the gold substrate. In the x - and y -directions, a periodic boundary condition was used. Embedded-atom method potential (EAM)⁵⁰ was employed to calculate interatomic potential in the gold substrate, and the atoms in the bottom layer were fixed.

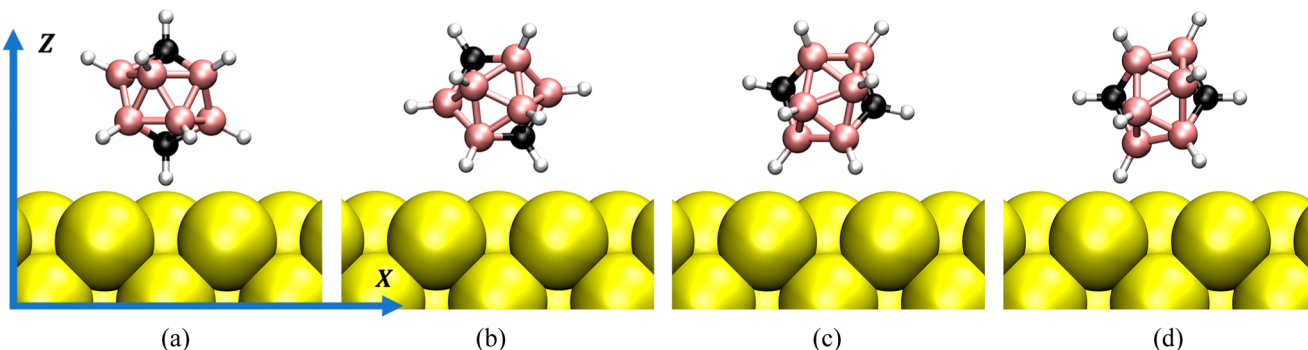


Figure 3. Major orientations of *p*-carborane on a gold surface. (a) One of the carbon atoms is closest to the gold surface, henceforth called C-down. (b) A carbon and two boron atoms are closest to the gold surface, henceforth called C–B–B-down. (c) Three boron atoms are closest to the gold surface, henceforth called B–B–B-down. (d) The line passing through the carbon atoms is parallel to the gold surface, henceforth called C-axe.

Table 3. Minimum and Maximum of Minimum PES, Their Corresponding Distance between *p*-Carborane and the Gold Substrate, and the Jump Barrier between Two Adjacent Cells for Each Major Orientation

orientation	energy (eV)		height (Å)		jump barrier	
	min	max	min	max	(eV)	(Å)
C-down	-0.557	-0.311	4.267	5.110	-0.416	4.681
C–B–B-down	-0.495	-0.396	4.472	4.813	-0.451	4.616
B–B–B-down	-0.472	-0.381	4.568	4.896	-0.428	4.715
C-axe	-0.483	-0.338	4.527	5.064	-0.413	4.757

Despite vast electronic structure calculation, only a few force fields have been developed for classical modeling of *p*-carborane intramolecular potential.^{51–53} Most notably, Allinger and co-workers developed the MM3 force field for 12-vortex boranes, carboranes, and their derivatives,⁵³ which we used in this paper to model the *p*-carborane intramolecular potential. The MM3 potential was first proposed for the conformational analysis of small organic molecules and hydrocarbons.^{54–56} It can also be used to estimate the energies and equilibrium structures with almost an experimental accuracy. Allinger found that coefficients of torsional potential including hydrogen or another atom of the substituent attached to the *p*-carborane cage are zero.⁵³ Thus, it is expected that in the gaseous phase of a nanocar, the rotation of the wheels would not be severely inhibited because of its bond to the chassis. Other limitations, especially the effect of substrate on rotation, will be considered as well.

The potential between *p*-carborane and gold was calculated using eqs 1 and 2, and Table 2 shows the LJ parameters used. Also, a cutoff radius of 15 Å and neighbor cutoff distance of 18 Å were used for the MD simulations.

3. RESULTS AND DISCUSSION

The details of modeling and simulation of *p*-carborane molecules on a gold surface were explained in the previous section. In this section, the results of PES and MD simulations are presented and compared.

3.1. Potential Energy Approach. PESs provide a quantitative approach for analyzing the motion of molecules on surfaces.^{57–61} In this section, we aim to find the most stable configuration for the *p*-carborane at different orientations and positions on the gold surface. The motion of *p*-carborane on gold substrate consists of two independent parts: transitional movement (sliding) and rotation. It can be predicted which part of the motion is more probable and dominant at a certain

condition. Because of its complex structure, carborane can have several major orientations on the substrate.

We first studied the sliding motion of *p*-carborane. The *p*-carborane molecule moved rigidly on the *x*–*y* plane above the substrate. At each point, the distance between the substrate and *p*-carborane was adjusted to minimize the potential energy. To find the minimum of the potential energy, a line search algorithm was employed until the change in potential energy was less than 1×10^{-5} eV. It should be noted that the orientation and internal coordinates of the molecule were kept steady during sliding. The PES depends heavily on the orientation of *p*-carborane. Several orientations were chosen, and the potential energy variation was calculated separately for each. Our choice of major orientations was tested by a series of PES calculations and then compared together. As demonstrated in Figure 3, the four major orientations were defined as follows.

- C-down: one of the carbon atoms is closest to the gold surface
- C–B–B-down: a carbon and two boron atoms are closest to the gold surface
- B–B–B-down: three boron atoms are closest to the gold surface
- C-axe: the line passing through the carbon atoms is parallel to the gold surface

We are most interested in the C-axe orientation because it is the orientation of *p*-carborane wheels in the nanocars. Because the carbon–gold interaction potential well (ϵ_{C-Au}) is deeper than the boron one (ϵ_{B-Au}), the system is generally more stable when one carbon atom is closer to the substrate or when several boron atoms are equally close to the substrate. (For details of the variation of potential energy during the sliding motion on gold for these four major orientations, see Figure S1 in the Supporting Information.) The results show the minimum PES at a every point on the gold surface, which is more useful data than a method of finding the PES at several fixed distances from the substrate as reported in refs 59 and 60. Obviously, the

distance between substrate and *p*-carborane corresponding to the minimum of potential energy is correlated with the minimum potential energy through the LJ potential (see eq 1). Thus, in the rest of this section, the minimum potential energy surface will be reported. Table 3 shows the minimum and maximum of minimum potential energy surface and their corresponding distance for each orientation.

We are most interested in the stable configurations. In Figure 4 we illustrate the variation of the minimum PES during the

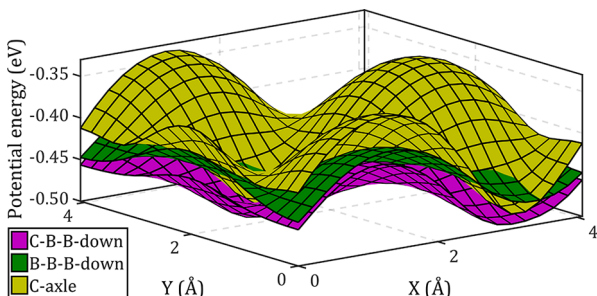


Figure 4. Variation of minimum PES of *p*-carborane during sliding motion on gold for C–B–B-down, B–B–B-down, and C-axe orientations.

sliding motion for C–B–B-down, B–B–B-down, and C-axe orientations together. At each point on the surface, the potential energy in the C–B–B-down orientation is lower than the potential energy in the B–B–B-down and C-Axe orientations. Also, the energy in the B–B–B-down orientation is often lower than that in the C-axe orientation. Therefore, the C–B–B-down orientation is more stable than the two other mentioned orientations. For this reason, in Figure 5 the variation of potential energy for C-down and C–B–B-down orientations are compared to find which is more stable.

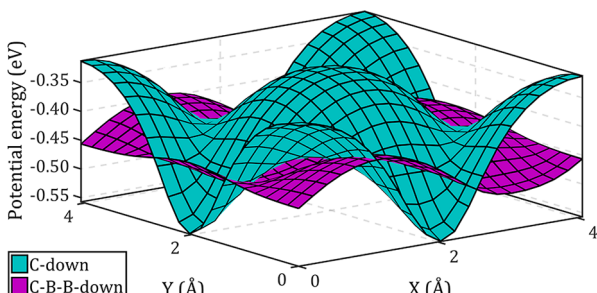


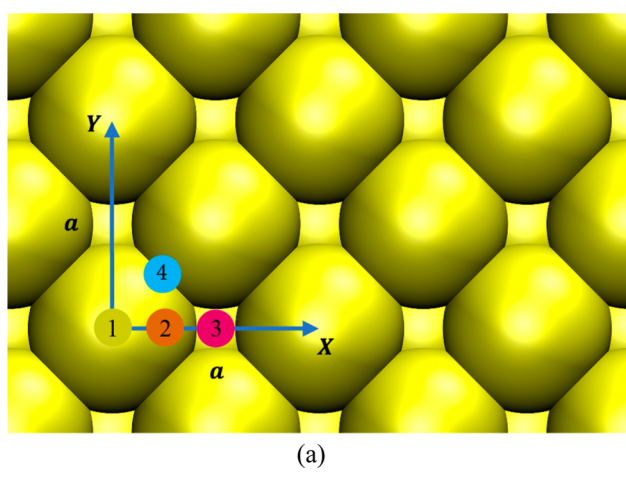
Figure 5. Variation of minimum PES of *p*-carborane during sliding motion on gold for C-down and C–B–B-down orientations.

Figure 5 shows that the variation of minimum PES in the C-down orientation is higher than the C–B–B-down orientation. Therefore, pure sliding motion in the C-down orientation requires higher kinetic energy compared to the C–B–B-down orientation. Although the C-down orientation has deeper potential wells, the C–B–B-down configuration is generally more stable in wide areas. Because of these deep potential wells, at low temperatures where the kinetic energy is insufficient, the C-down orientation is more probable and *p*-carborane tends not to change its orientation at these wells. However, sliding to an adjacent potential minima is not extremely confined because of the presence of high-energy maxima. Figures 4 and 5 demonstrate that moving between potential minima does not

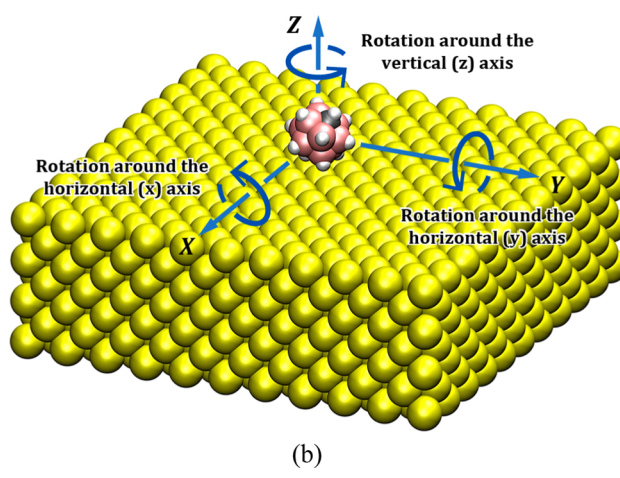
require reaching the maximum energy level. Alternative paths exist in the form of saddle points in the potential energy plot which enable the molecule to slide at a lower energy. These saddle points are the least energy-intensive paths of sliding. The energy of these points and their corresponding separation distance are shown in Table 3 as jump barrier energy. The C–B–B-down orientation has the lowest jump barrier of −0.451 eV (see Table 3), thus, the likelihood of pure sliding is higher in this configuration in comparison with the C-down and C-axe configuration. However, because the minimum barrier sliding path in the C–B–B-down orientation is close to the intersection of C-down and C–B–B-down PESs, the molecule may rotate to a C-down orientation and drop into its deep potential well.

Next we study the rotation of *p*-carborane molecules on a Au(001) surface using the potential energy approach. The potential energy variation was calculated for rotation around a horizontal and vertical axes. For rotation around the horizontal axis, two different scenarios were studied. In the first scenario, the molecule was rotated around the *y*-axis from a C-axe orientation, reaching B–B–B-down, C–B–B-down, and C-down orientations successively. In the second scenario, the molecule in the C-axe orientation was rotated around the C–C axle (*x*-axis). At each step, the distance between the center of mass of the molecule and substrate was adjusted as before to minimize the potential energy. Because the potential energy depends heavily on the lateral position of the *p*-carborane center of mass relative to the crystalline structure of the gold substrate, the calculations were performed separately for four key positions on the substrate: point 1, (0, 0); point 2, (a/4, 0); point 3, (a/2, 0); and point 4, (a/4, a/4). Figure 6 shows these positions and rotation axes on the gold crystal structure. The horizontal position of the center of mass of the *p*-carborane molecule was set to one of the mentioned positions and kept constant during rotation.

As in the first scenario, the variation of potential energy is plotted in Figure 7 with the *p*-carborane rotating around the *y*-axis. It is evident that rotation from the C-axe to the B–B–B-down orientation reduces the potential energy and does not have a barrier. Therefore, in the absence of external constraints, *p*-carborane in a C-axe orientation will always rotate to reach the B–B–B-down orientation. The rotation from the B–B–B-down to the C–B–B-down orientation makes the system more stable as well. However, unlike the previous case, the molecule must have enough kinetic energy to overcome the barrier, otherwise the molecule tends to remain in the local potential energy minima unless enough energy is acquired to perform the rotation. These energy barriers depend on the position, and the rotation is more probable at positions where the barrier is low. The change in the potential energy during rotation from C–B–B-down to C-down orientation is different because the potential increases at all positions except for point 3. At this point no barrier exists, and the rotation will occur without a hurdle. Comparing Table 3 and Figure 7 reveals that the energy barrier for rotation around a horizontal axis (*y*-axis) is generally higher than for pure sliding. Thus, it can be predicted that *p*-carborane tends to slide rather than rotate. Also, it is worth noting that the rotational motion will mainly consist of C–B–B-down to another C–B–B-down at points 1, 2, and 4 or to the C-down orientation at point 3. It should be emphasized that we only predict the possibility of some kind of motion or its dominance and we are not going to indicate that moving to an adjacent cell minima is limited to a specific path.



(a)



(b)

Figure 6. Potential energy calculations during rotational motion were performed separately for the four key positions on the horizontal gold surface. (a) The positions are point 1, $(0, 0)$; point 2, $(a/4, 0)$; point 3, $(a/2, 0)$; and point 4, $(a/4, a/4)$, where a is the lattice constant of gold. (b) The rotation axes are denoted.

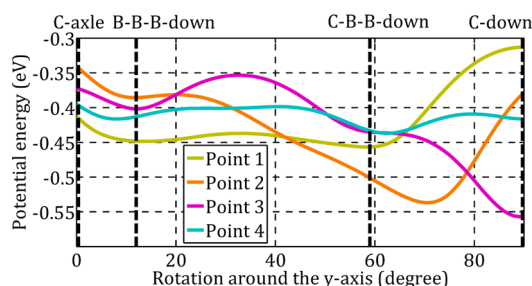


Figure 7. Variation of the minimum potential energy when rotating around the y -axis from the C-axe orientation, reaching B–B–B-down, C–B–B-down, and C-down orientations successively on gold surface at the four key positions as shown in Figure 6a.

The second scenario is made up of rotation around the C–C axle. In this case, the molecule remains in the C-axe orientation during rotation around the x -axis. Similar to the previous scenario, the separation distance between the *p*-carborane and gold surface is optimized at each orientation to minimize the potential energy. This mode of rotation represents the rotation of the *p*-carborane as a nanocar wheel; therefore, it is a subject of our interest. The potential energy calculations were performed at the same four key positions shown in Figure 6a, and the results are plotted in Figure 8. Also, it should be noted that this assumption is an approximation because the chassis of nanocars are generally flexible, and the C–C axis would not remain consistent with the x -axis; the bond between *p*-

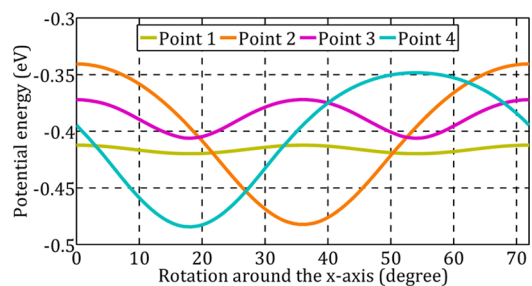


Figure 8. Variation of *p*-carborane potential energy when rotating around the x -axis in the C-axe configuration for the four key positions as shown in Figure 6a.

carborane and chassis tends to bend toward the more stable B–B–B-down orientation. According to Figure 8, the variation of potential energy during rotation around the x -axis is between 2% and 34% depending on the position of center of mass of *p*-carborane relative to the gold crystalline structure. The minimum of the energy barrier in this rotation scenario (-0.412 eV) is higher than the maximum of the pure sliding motion barrier (see Table 3). Thus, sliding is more probable to occur, and we predict that the *p*-carborane will not rotate continuously as a nanocar wheel.

The other possible rotational motion scenario is rotation around the vertical axis (z -axis). Figures 9a and 9b show the variation of potential energy for rotation around a vertical axis in C-down and C-axe orientations at each of the mentioned key positions, respectively. The variation is extremely small for the C-down orientation; thus, *p*-carborane would freely rotate around the vertical axis in this orientation. According to Figure 5, the deepest potential wells belong to the C-down orientation. At low temperatures, *p*-carborane would get trapped in these wells (C-down orientation), and in this case the motion would mainly consist of rotation around the vertical axis because there is no energy barrier to prevent its rotation. As demonstrated in section 3.2, even at higher temperatures this rotation around the vertical axis occurs easier than any rotation around the horizontal one. Despite this, as shown in Figure 9b, the energy barrier is high for rotation around a vertical axis in the C-axe orientation, and at most positions, *p*-carborane tends to slide instead of rotate in this configuration.

In this section, we analyzed the potential energy of *p*-carborane and its variation during sliding and rotation on a gold substrate. With this information, the physics behind the motion of *p*-carborane can be better understood. The potential energy method may be used to predict the motion of *p*-carborane in different environments and in the structure of a nanocar.

3.2. Molecular Dynamics Approach. In this section, we study the motion of *p*-carborane on a gold surface using the classical MD method. The details of modeling and simulation of *p*-carborane molecules on a gold surface were explained in section 2.2. The *p*-carborane motion was simulated at different temperatures and bulk parameters, e.g., temperature and potential energy, and *p*-carborane status parameters, i.e., position, speed, and angular velocity, were recorded every 100 fs. The simulation was conducted for 8 ns, and the position

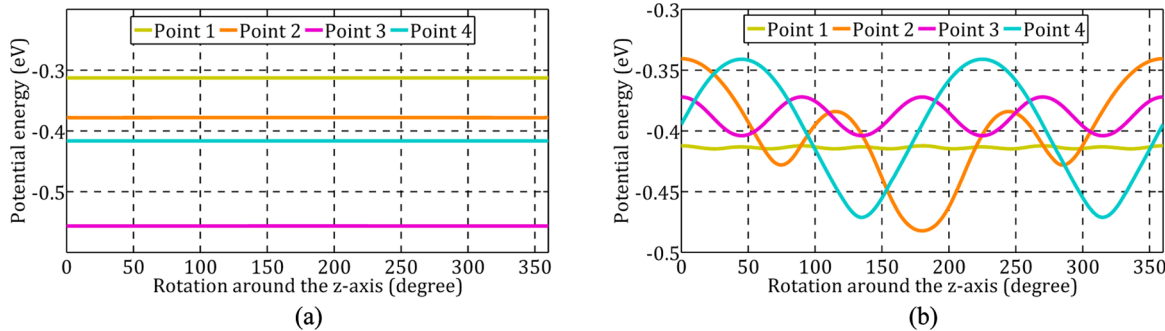


Figure 9. Variation of *p*-carborane potential energy when rotating around the *z*-axis in (a) C-down and (b) C-axle configuration for four key positions as shown in Figure 6a.

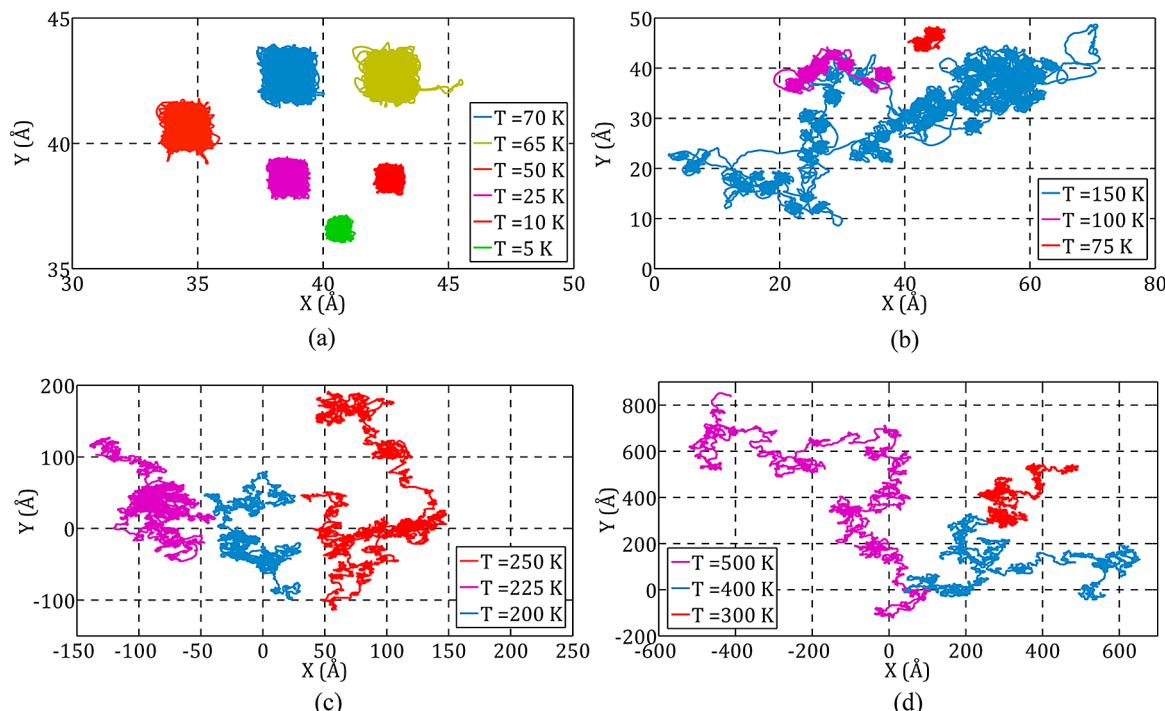


Figure 10. Trajectory of *p*-carborane on the gold surface versus temperature. (a) The *p*-carborane is trapped in a cell at 70 K and lower temperatures. (b) The *p*-carborane jumps to adjacent cells at 75 K, and the number of jumps increases as the temperature rises. (c) The frequency and range of jumps of *p*-carborane increases at 200 K. (d) The *p*-carborane experiences free continuous motion on the gold substrate at high temperatures.

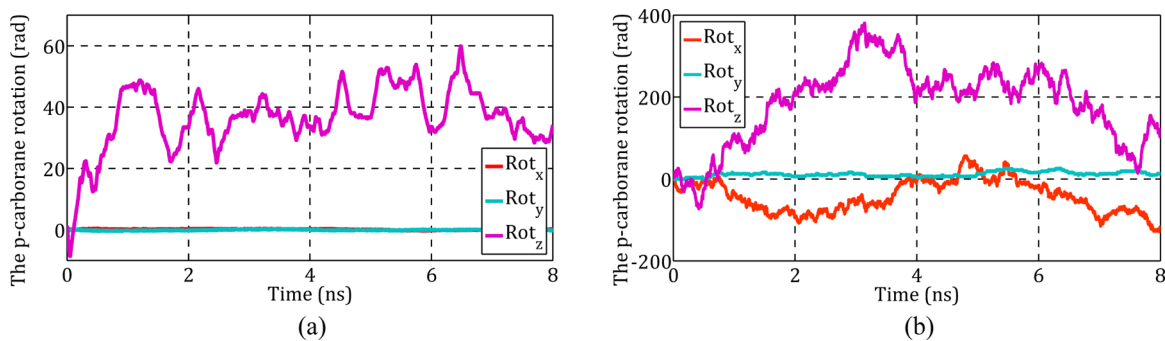


Figure 11. Rotation of the *p*-carborane around the *x*-, *y*-, and *z*-axes (a) at 5 K and (b) 500 K.

of all atoms was recorded every 2 ps. Thus, 80 000 data points were recorded. Figure 10 shows the trajectories of *p*-carborane at different temperatures. It is evident that the regime of motion depends on the temperature. Below 75 K, *p*-carborane is trapped in the crystal structure of gold and cannot leave the

potential minimum it is positioned in (see Figure 10a). When the temperature reaches 75 K, the molecule starts jumping to adjacent cells. The motion at temperatures between 75 and 200 K consists of a series of occasional jumps between potential minima. As shown in Figure 10b, the motion is not continuous

at these temperatures. The frequency and range of the jumps increase with the temperature (see Figures 10b and 10c). Above 250 K the motion becomes continuous and the speed of motion increases with temperature. As shown in Figure 10d, the motion is completely continuous at 400 and 500 K, and finally all the MD simulations above 500 K resulted in desorption of the *p*-carborane from the substrate.

We stated in section 3.1 that at low temperatures, *p*-carborane gets trapped in a potential well at the C-down orientation because it does not have enough energy to escape. Also, rotation around the *z*-axis is the dominant mode of motion because there is no energy barrier preventing it. Figure 11 shows rotation around the *x*, *y*, and *z*-axis at 5 and 500 K. As shown in Figure 11a, at 5 K the *p*-carborane molecule may rotate around the *z*-axis for 40 rad in a short interval; however, it did not experience transitional motion or rotation around the horizontal axis. However, the RMS of angular velocity at this temperature is $[\omega_x \omega_y \omega_z]_{\text{RMS}} = [0.899 \ 0.898 \ 0.877]$. This calculation was performed for different temperatures, where the rotation may reach 400 rad around the *z*-axis and -100 rad around the *x*-axis at 500 K (see Figure 11b). At 5 K, translation is less than 2 Å (see Figure 10a), while at 500 K, *p*-carborane slides approximately 1000 Å. Thus, it can be concluded that at low temperatures where the kinetic energy is insufficient *p*-carborane gets trapped in a potential well, and rotation around the *z*-axis is the dominant mode of motion. Also, the results demonstrate that rotation around the horizontal axis is more difficult than a sliding motion.

The LJ interaction between the *p*-carborane molecule and the gold substrate was recorded in MD simulations. Average, standard deviation, minimum, and maximum potential energy at different temperatures are plotted in Figure 12. Using the

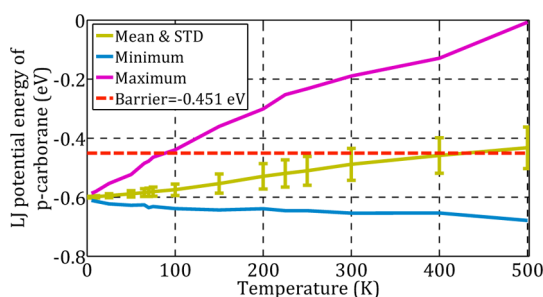


Figure 12. Average, standard deviation, minimum, and the maximum of LJ interaction between the *p*-carborane molecule and gold substrate obtained in MD simulation as a function of temperature.

PES approach we found that in order for the *p*-carborane to slide on the gold surface its potential energy level must reach -0.451 eV, corresponding to 4.616 Å separation distance. As shown in Figure 12, the molecule reaches this potential level of energy between 70 and 75 K. Because 75 K was the temperature the first sliding motions were observed in MD simulations, the results from classical MD calculation and PES approaches are in good agreement. All MD simulations above 500 K, even with different initial conditions, resulted in the separation of *p*-carborane from the substrate. Figure 12 shows that at 500 K LJ potential significantly decreases and its value reaches 0.007 eV. It was observed that increasing the simulation time at 500 K resulted in the separation of *p*-carborane from the substrate. The reason for this behavior might be high-energy impacts from gold substrate to *p*-carborane molecule,

where the van der Waals force is not sufficient to keep the molecule on the surface.

In order to better understand the variation of LJ interactions between *p*-carborane and a gold substrate, a probability of powerful jumps of the molecule between potential minima is shown in Figure 13 versus temperature. The powerful jump of

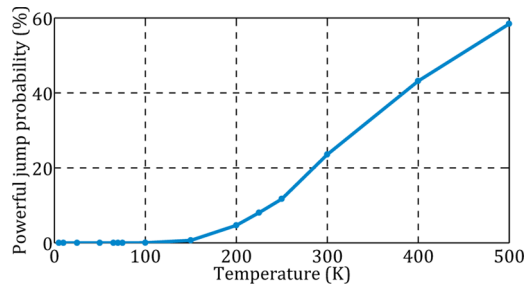


Figure 13. Variation of the *p*-carborane probability of powerful jumps as a function of the temperature.

p-carborane is defined as a jump in which the molecule has a certain level of energy (-0.451 eV) to jump to an adjacent cell. This is calculated by comparing the number of times in which the *p*-carborane molecule has sufficient energy to jump to the total number of time steps. It should be noted that the molecule does not necessarily jump when the potential energy is sufficient. To perform a jump, *p*-carborane must also have enough horizontal momentum. As demonstrated in Figure 13, this probability increases with temperature. It can be revealed that it is nearly impossible for *p*-carborane to jump to adjacent cells below 70 K; therefore, the probability is close to zero.

The change of motion regime was studied qualitatively. To analyze the motion regime of *p*-carborane on a gold surface, the transitional motion should be quantified. The average speed of *p*-carborane may provide us a better understanding of the motion regime. For this goal, the horizontal RMS speed of center of mass $v_{\text{RMS}} = \sqrt{\langle v_x^2 + v_y^2 \rangle}$ of the *p*-carborane was obtained from MD calculations, and the equipartition of energy⁶² are plotted as a function of temperature. (For details, see Figure S2 in the Supporting Information.) It can be concluded that the RMS speed of the *p*-carborane is mainly the result of temperature-induced vibrations, and translation motion (including hopping and continuous motion) is a very small part of the overall motion or kinetic energy. Thus, v_{RMS} cannot provide an evaluation criteria for the translational motion regime as a result of temperature and did not show extra information.

As an alternative method, the mean square displacement (MSD) is the standard parameter used to describe a diffusive motion of the particles. Then, the diffusion coefficient can be obtained from the MSD plot. MSD describes the amount of system explored during a random walk and usually applies to a system of numerous particles. However, some estimators for MSD of a single particle have been reported in refs 63 and 64. Here, we use the following definition of mean square displacement:

$$\text{MSD}(i\Delta t) = \langle |\mathbf{r}_i - \mathbf{r}_0|^2 \rangle \quad (3)$$

where $\langle \rangle$ represents averaging over all particles; \mathbf{r}_i is the position vector of the *p*-carborane center of mass at step *i*, and

Δt is the time step. Diffusion coefficient (D) is defined as the slope of the MSD as

$$D = \lim_{i \rightarrow N} \frac{\text{MSD}}{4(i\Delta t)^\alpha} \quad (4)$$

for two-dimensional diffusion, where α is the anomaly parameter and N is the length of data points. In a normal diffusion, e.g., Brownian dynamic, $\alpha = 1$. The MSD parameter is a good indicator of the motion of the particles, and many properties of the system, e.g., confinements, can be found using it. Ernst and Kohler proposed a novel method for calculating the diffusion coefficient of a protein on a substrate.⁶⁵ In this method, they captured a very long trajectory of N_T data points. They then divide the full trajectory into equal segments that are treated as individual trajectories of shorter length. The length of these segments are denoted as N_{seg} . In this manner, an ensemble of N_T/N_{seg} short trajectories or imaginary particles is formed. This enabled an analysis of the obtained MSD curves, and as a consequence, the diffusion coefficient D is then found by averaging the segments using eqs 3 and 4.

Here, the full trajectory was divided into 80 equal segments of $N_{\text{seg}} = 1000$ data points each, and the diffusion coefficient D was calculated for an ensemble of 79 trajectories (The first segment is neglected for relaxation of simulation). An Arrhenius analysis of the diffusion coefficient is presented to better understand the variation of the diffusion coefficient of *p*-carborane on the gold substrate as a function of temperature. The Arrhenius equation⁶⁶ is a simple yet accurate model of the dependence of reaction rate on temperature.

$$D = Ae^{-E_a/K_B T} \quad (5)$$

where A is a prefactor and E_a is the activation energy per molecule of process or reaction. It is usually derived experimentally for the temperature-induced processes, and it can be used to describe the temperature dependence of the diffusion coefficient. Figure 14 depicts the diffusion coefficient

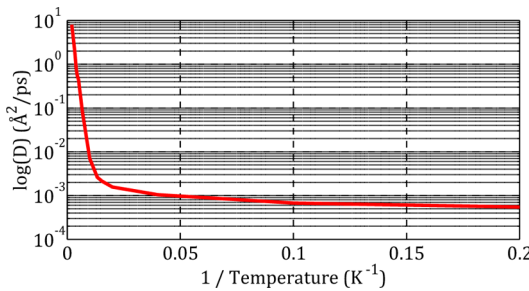


Figure 14. Arrhenius plot of the diffusion coefficient of *p*-carborane on the gold surface.

on a logarithmic scale [$\log(D)$] as a function of the reciprocal of temperature. It is evident that the diffusion coefficient increases with temperature. Figure 14 demonstrate that below 75 K the diffusion coefficient has a slight slope for temperatures. Therefore, in this region the motion is not affected by the temperature. At a temperature of 75 K, the slope of the MSD curve significantly changes. This corresponds to the change in motion regime. When the temperature is increased, the slope of the diffusion coefficient becomes much steeper, indicating that the *p*-carborane moves on the surface freely. This plot does not show a clear change in motion regime at temperatures above 100 K.

The change in motion regime demonstrated in Figure 10 is mainly the result of the translational motion of *p*-carborane on the substrate, not its atoms vibrations. Thus, the distance traveled by the *p*-carborane molecule between potential minima is a better parameter for describing the regime of motion than RMS speed or diffusion coefficient. The presented heuristic method acts as a filter omitting vibrational motion in the cell. The length of jumps is calculated as follows.

$$\text{p-carborane jumps} = \frac{a}{2} \sum_{i=0}^{N-1} \left\| \left\lfloor \frac{2\mathbf{r}_{i+1}}{a} \right\rfloor - \left\lfloor \frac{2\mathbf{r}_i}{a} \right\rfloor \right\| \quad (6)$$

where $\|\cdot\|$ represents the L^2 norm of vector and $\lfloor \cdot \rfloor$ is the nearest integer function. Figure 15 shows the number of lattice

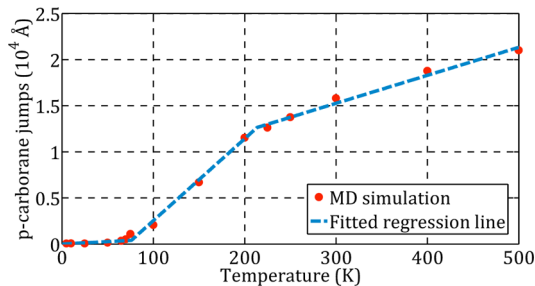


Figure 15. Effect of temperature on the rate of *p*-carborane lattice jumps.

jumps as a function of temperature. It can be seen that below 75 K *p*-carborane is immobile. Although small jumps may occur at this temperature range, these jumps do not have enough energy to move the molecule to another cell. Above 75 K, *p*-carborane starts jumping to the adjacent cell and the number of jumps increases with the temperature. Between 75 and 200 K, the dominant regime of motion is discontinuous, jumping multiple cells at once. Between 200 and 250 K, the regime of motion starts to change into a continuous mode. At 400 K, the motion is entirely continuous. It is evident that the change of slope in this curve corresponds to the change in the regime of motion.

4. CONCLUSIONS

In this paper we studied the mobility of *p*-carborane on gold substrate using the PES approach and classical MD method. In the PES approach (section 3.1), sliding and rotational motions were studied on the Au(001) separately. It was found that depending on the position of the *p*-carbonate molecule on the substrate, the most stable orientation is either C-down or C-B-B-down. The C-B-B-down orientation has the lowest energy barrier for sliding motion, -0.451 eV. Thus, pure sliding motion would probably occur in this orientation. The PES of *p*-carborane during rotation of *p*-carborane around a horizontal and vertical axis was also calculated, and the energy levels were found. It was demonstrated that *p*-carborane would freely rotate around the vertical axis in the C-down orientation and that the rotation around the horizontal axis has an energy barrier larger than that of pure sliding. On the other hand, it was found that the *p*-carborane molecule on a Au(111) surface experiences a smoother PES compared to a Au(001) surface. Thus, it can be predicted that the *p*-carborane starts sliding at lower temperatures on Au(111) in comparison with Au(001). The C-B-B-down orientation on Au(111) has the lowest jump barrier of -0.511 eV in comparison with Au(001), which was -0.451 eV

(see Figures S3–S6, Table S1, and related discussion in the Supporting Information). It should be noted that the motion of the *p*-carborane is highly influenced by the temperature-induced vibrations of the substrate atoms. This result indicates that the motion is random in general. Therefore, finding a precise minimum-energy path of transitions between two specific configurations, and predicting the occurrence of such kinds of trajectories, may not be practicable.

In section 3.2, the system was simulated using classical MD at different temperatures from 5 to 500 K. It was found that *p*-carborane could rotate around the vertical axis even at low temperatures, but rotation around the horizontal axis is confined. These results are in perfect agreement with the PES results. To better understand the change of motion regime of *p*-carborane, we also proposed a quantified parameter for describing the motion. When the temperature reaches 500 K, the system becomes unstable, and given enough time, a separation between *p*-carborane and substrate occurs. It was shown that below 75 K *p*-carborane is immobile. While at 75 K, the molecule starts to jump and the length of the jumps increases with temperature. Discontinuous jumps are the dominant regime of motion for temperatures between 75 and 200 K. Above 200 K the motion is mostly continuous.

The results of this study can help us choose the best material for their application. The analytical results provide a good reference for performing experiments. Many aspects of the motion of *p*-carborane on gold can be predicted with these methods, reducing the number of required experiments.

ASSOCIATED CONTENT

Supporting Information

The Supporting Information is available free of charge on the ACS Publications website at DOI: [10.1021/acs.jpcc.6b02201](https://doi.org/10.1021/acs.jpcc.6b02201).

Details of the variation of potential energy during the sliding motion on gold for the four major orientations (Figure S1), implementation of the equipartition of energy (Figure S2), and discussion about the effect of different FCC crystalline directions on the PES (Figures S3–S6 and Table S1) ([PDF](#))

AUTHOR INFORMATION

Corresponding Authors

*E-mail: sm_hlavasani@mech.sharif.edu.

*E-mail: nejat@sharif.edu. Phone: +98 21 6616 5543.

*E-mail: meghdari@sharif.edu.

Notes

The authors declare no competing financial interest.

ACKNOWLEDGMENTS

The authors thank the Iranian National Science Foundation (INSF) and the Iranian Nanotechnology Initiative Council (INIC) for their invaluable support. We are grateful to the Center of Excellence in Design, Robotics and Automation (CEDRA) of Sharif University of Technology for providing computational resources for this research.

REFERENCES

- Kay, E. R.; Leigh, D. A.; Zerbetto, F. Synthetic molecular motors and mechanical machines. *Angew. Chem., Int. Ed.* **2007**, *46*, 72–191.
- Feynman, R. P. There's Plenty of Room at the Bottom. *Eng. Sci.* **1960**, *23*, 22–36.
- Shinkai, S.; Nakaji, T.; Nishida, Y.; Ogawa, T.; Manabe, O. Photoresponsive crown ethers. 1. Cis-trans isomerism of azobenzene as a tool to enforce conformational changes of crown ethers and polymers. *J. Am. Chem. Soc.* **1980**, *102*, 5860–5865.
- Vives, G.; Tour, J. M. Synthesis of Single-Molecule nanocars. *Acc. Chem. Res.* **2009**, *42*, 473–487.
- Shirai, Y.; Osgood, A. J.; Zhao, Y.; Kelly, K. F.; Tour, J. M. Directional control in thermally driven single-molecule nanocars. *Nano Lett.* **2005**, *5*, 2330–2334.
- Shirai, Y.; Morin, J. F.; Sasaki, T.; Guerrero, J. M.; Tour, J. M. Recent progress on nanovehicles. *Chem. Soc. Rev.* **2006**, *35*, 1043–1055.
- Shirai, Y.; Osgood, A. J.; Zhao, Y.; Yao, Y.; Saudan, L.; Yang, H.; Yu-Hung, C.; Alemany, L. B.; Sasaki, T.; Morin, J. F.; Guerrero, J. M.; Kelly, K. F.; Tour, J. M. Surface-rolling molecules. *J. Am. Chem. Soc.* **2006**, *128*, 4854–4864.
- Morin, J. F.; Sasaki, T.; Shirai, Y.; Guerrero, J. M.; Tour, J. M. Synthetic routes toward carborane-wheeled nanocars. *J. Org. Chem.* **2007**, *72*, 9481–9490.
- Sasaki, T.; Tour, J. M. Synthesis of a dipolar nanocar. *Tetrahedron Lett.* **2007**, *48*, 5821–5824.
- Vives, G.; Kang, J.; Kelly, K. F.; Tour, J. M. Molecular machinery: synthesis of a "nanodragster". *Org. Lett.* **2009**, *11*, 5602–5605.
- Vives, G.; Tour, J. M. Synthesis of a nanocar with organometallic wheels. *Tetrahedron Lett.* **2009**, *50*, 1427–1430.
- Chu, P.-L. E.; Wang, L.-Y.; Khatua, S.; Kolomeisky, A. B.; Link, S.; Tour, J. M. Synthesis and Single-Molecule Imaging of Highly Mobile Adamantane-Wheeled Nanocars. *ACS Nano* **2013**, *7*, 35–41.
- Sasaki, T.; Morin, J. F.; Lu, M.; Tour, J. M. Synthesis of a single-molecule nanotruck. *Tetrahedron Lett.* **2007**, *48*, 5817–5820.
- Sasaki, T.; Guerrero, J.; Leonard, A.; Tour, J. Nanotrains and self-assembled two-dimensional arrays built from carboranes linked by hydrogen bonding of dipyridones. *Nano Res.* **2008**, *1*, 412–419.
- Sasaki, T.; Guerrero, J. M.; Tour, J. M. The assembly line: self-assembling nanocars. *Tetrahedron* **2008**, *64*, 8522–8529.
- Van Delden, R. A.; Ter Wiel, M. K. J.; Pollard, M. M.; Vicario, J.; Koumura, N.; Feringa, B. L. Unidirectional molecular motor on a gold surface. *Nature* **2005**, *437*, 1337–1340.
- Morin, J. F.; Shirai, Y.; Tour, J. M. En route to a motorized nanocar. *Org. Lett.* **2006**, *8*, 1713–1716.
- Kudernac, T.; Ruangsrapichat, N.; Parschau, M.; MacIá, B.; Katsonis, N.; Harutyunyan, S. R.; Ernst, K. H.; Feringa, B. L. Electrically driven directional motion of a four-wheeled molecule on a metal surface. *Nature* **2011**, *479*, 208–211.
- Sasaki, T.; Tour, J. M. Synthesis of a new photoactive nanovehicle: A nanoworm. *Org. Lett.* **2008**, *10*, 897–900.
- Claytor, K.; Khatua, S.; Guerrero, J. M.; Tcherniak, A.; Tour, J. M.; Link, S. Accurately determining single molecule trajectories of molecular motion on surfaces. *J. Chem. Phys.* **2009**, *130*, 164710–164718.
- Khatua, S.; Guerrero, J. M.; Claytor, K.; Vives, G.; Kolomeisky, A. B.; Tour, J. M.; Link, S. Micrometer-Scale Translation and Monitoring of Individual Nanocars on Glass. *ACS Nano* **2009**, *3*, 351–356.
- Wang, L.-L.; Cheng, H.-P. Density functional study of the adsorption of a C₆₀ monolayer on Ag(111) and Au(111) surfaces. *Phys. Rev. B: Condens. Matter Mater. Phys.* **2004**, *69*, 165417.
- Hamada, I.; Tsukada, M. Adsorption of C₆₀ on Au(111) revisited: A van der Waals density functional study. *Phys. Rev. B: Condens. Matter Mater. Phys.* **2011**, *83*, 245437.
- Nejat Pishkenari, H.; Nemati, A.; Meghdari, A.; Sohrabpour, S. A close look at the motion of C₆₀ on gold. *Curr. Appl. Phys.* **2015**, *15*, 1402–1411.
- Akimov, A. V.; Nemukhin, A. V.; Moskovsky, A. A.; Kolomeisky, A. B.; Tour, J. M. Molecular dynamics of surface-moving thermally driven nanocars. *J. Chem. Theory Comput.* **2008**, *4*, 652–656.
- Konyukhov, S. S.; Kupchenko, I. V.; Moskovsky, A. A.; Nemukhin, A. V.; Akimov, A. V.; Kolomeisky, A. B. Rigid-body

- molecular dynamics of fullerene-based nanocars on metallic surfaces. *J. Chem. Theory Comput.* **2010**, *6*, 2581–2590.
- (27) Akimov, A. V.; Kolomeisky, A. B. Unidirectional rolling motion of nanocars induced by electric field. *J. Phys. Chem. C* **2012**, *116*, 22595–22601.
- (28) Darvish Ganji, M.; Ghorbanzadeh Ahangari, M.; Emami, S. M. Carborane-wheeled nanocar moving on graphene/graphyne surfaces: van der Waals corrected density functional theory study. *Mater. Chem. Phys.* **2014**, *148*, 435–443.
- (29) Tillekaratne, A.; Siap, D.; Trenary, M. Adsorption and Dehydrogenation of Ortho-Carborane on the Pt(111) Surface. *J. Phys. Chem. C* **2008**, *112*, 8682–8689.
- (30) Zeng, H.; Byun, D.; Zhang, J.; Vidali, G.; Onellion, M.; Dowben, P. A. Adsorption and bonding of molecular icosahedra on Cu(100). *Surf. Sci.* **1994**, *313*, 239–250.
- (31) Caruso, A. N.; Bernard, L.; Xu, B.; Dowben, P. A. Comparison of Adsorbed Orthocarborane and Metacarborane on Metal Surfaces. *J. Phys. Chem. B* **2003**, *107*, 9620–9623.
- (32) von Wrochem, F.; Scholz, F.; Gao, D.; Nothofer, H.-G.; Yasuda, A.; Wessels, J. M.; Roy, S.; Chen, X.; Michl, J. High-Band-Gap Polycrystalline Monolayers of a 12-Vertex p-Carborane on Au(111). *J. Phys. Chem. Lett.* **2010**, *1*, 3471–3477.
- (33) Scholz, F.; Nothofer, H.-G.; Wessels, J. M.; Nelles, G.; von Wrochem, F.; Roy, S.; Chen, X.; Michl, J. Permethylated 12-Vertex p-Carborane Self-Assembled Monolayers. *J. Phys. Chem. C* **2011**, *115*, 22998–23007.
- (34) Kupchenko, I. V.; Moskovsky, A. A.; Nemukhin, A. V.; Kolomeisky, A. B. On the Mechanism of Carborane Diffusion on a Hydrated Silica Surface. *J. Phys. Chem. C* **2011**, *115*, 108–111.
- (35) Valiev, M.; Bylaska, E. J.; Govind, N.; Kowalski, K.; Straatsma, T. P.; Van Dam, H. J. J.; Wang, D.; Nieplocha, J.; Apra, E.; Windus, T. L.; de Jong, W. A. NWChem: A comprehensive and scalable open-source solution for large scale molecular simulations. *Comput. Phys. Commun.* **2010**, *181*, 1477–1489.
- (36) Hermansson, K.; Wójcik, M.; Sjöberg, S. o-, m-, and p-Carboranes and Their Anions: Ab Initio Calculations of Structures, Electron Affinities, and Acidities†. *Inorg. Chem.* **1999**, *38*, 6039–6048.
- (37) Salam, A.; Deleuze, M. S.; François, J. P. Computational study of the structural and vibrational properties of ten and twelve vertex closo-carboranes. *Chem. Phys.* **2003**, *286*, 45–61.
- (38) Bohn, R. K.; Bohn, M. D. The molecular structures of 1,2-, 1,7-, and 1,12-dicarba-closo-dodecaborane (12), B₁₀C₂H₁₂. *Inorg. Chem.* **1971**, *10*, 350–355.
- (39) Touloudian, Y. S.; Kirby, R. K.; Taylor, R. E.; Desai, P. D. *Thermal expansion—Metallic elements and alloys*; IFI/Plenum: New York, 1975.
- (40) Dutta, B. N.; Dayal, B. Lattice Constants and Thermal Expansion of Gold up to 878 °C by X-Ray Method. *Phys. Status Solidi B* **1963**, *3*, 473–477.
- (41) Sheng, H. W.; Kramer, M. J.; Cadien, A.; Fujita, T.; Chen, M. W. Highly optimized embedded-atom-method potentials for fourteen fcc metals. *Phys. Rev. B: Condens. Matter Mater. Phys.* **2011**, *83*, 134118.
- (42) Heinz, H.; Vaia, R. A.; Farmer, B. L.; Naik, R. R. Accurate Simulation of Surfaces and Interfaces of Face-Centered Cubic Metals Using 12–6 and 9–6 Lennard-Jones Potentials. *J. Phys. Chem. C* **2008**, *112*, 17281–17290.
- (43) Gamba, Z.; Powell, B. M. The condensed phases of carboranes. *J. Chem. Phys.* **1996**, *105*, 2436–2440.
- (44) Lorentz, H. A. Ueber die Anwendung des Satzes vom Virial in der kinetischen Theorie der Gase. *Ann. Phys.* **1881**, *248*, 127–136.
- (45) Berthelot, D. Sur le mélange des gaz. *C. R. Hebd. Séances Acad. Sci.* **1898**, *126*, 1703 1857.
- (46) Plimpton, S. Fast Parallel Algorithms for Short-Range Molecular Dynamics. *J. Comput. Phys.* **1995**, *117*, 1–19.
- (47) Humphrey, W.; Dalke, A.; Schulten, K. VMD: visual molecular dynamics. *J. Mol. Graphics* **1996**, *14*, 33–38.
- (48) Nosé, S. A unified formulation of the constant temperature molecular dynamics methods. *J. Chem. Phys.* **1984**, *81*, 511–519.
- (49) Hoover, W. G. Canonical dynamics: Equilibrium phase-space distributions. *Phys. Rev. A: At., Mol., Opt. Phys.* **1985**, *31*, 1695–1697.
- (50) Daw, M. S.; Baskes, M. I. Embedded-atom method: Derivation and application to impurities, surfaces, and other defects in metals. *Phys. Rev. B: Condens. Matter Mater. Phys.* **1984**, *29*, 6443–6453.
- (51) Timofeeva, T. V.; Allinger, N. L.; Buehl, M.; Mazurek, U. Application of molecular mechanics for calculations of metallocarborane molecules. *Russ. Chem. Bull.* **1994**, *43*, 1795–1801.
- (52) Timofeeva, T. V.; Mazurek, U.; Allinger, N. L. Molecular mechanics calculations on carboranes and metallocarboranes. *J. Mol. Struct.: THEOCHEM* **1996**, *363*, 35–42.
- (53) Timofeeva, T. V.; Suponitsky, K. Y.; Yanovsky, A. I.; Allinger, N. L. The MM3 force field for 12-vertex boranes and carboranes. *J. Organomet. Chem.* **1997**, *536–537*, 481–488.
- (54) Allinger, N. L.; Yuh, Y. H.; Lii, J. H. Molecular mechanics. The MM3 force field for hydrocarbons. I. *J. Am. Chem. Soc.* **1989**, *111*, 8551–8566.
- (55) Lii, J. H.; Allinger, N. L. Molecular mechanics. The MM3 force field for hydrocarbons. 2. Vibrational frequencies and thermodynamics. *J. Am. Chem. Soc.* **1989**, *111*, 8566–8575.
- (56) Lii, J. H.; Allinger, N. L. Molecular mechanics. The MM3 force field for hydrocarbons. 3. The van der Waals' potentials and crystal data for aliphatic and aromatic hydrocarbons. *J. Am. Chem. Soc.* **1989**, *111*, 8576–8582.
- (57) Lohrasebi, A.; Neek-Amal, M.; Ejtehadi, M. R. Directed motion of C₆₀ on a graphene sheet subjected to a temperature gradient. *Phys. Rev. E* **2011**, *83*, 042601.
- (58) Savin, A. V.; Kivshar, Y. S. Transport of fullerene molecules along graphene nanoribbons. *Sci. Rep.* **2012**, *2*, 1012.
- (59) Jafary-Zadeh, M.; Reddy, C.; Sorkin, V.; Zhang, Y.-W. Kinetic nanofriction: a mechanism transition from quasi-continuous to ballistic-like Brownian regime. *Nanoscale Res. Lett.* **2012**, *7*, 148.
- (60) Jafary-Zadeh, M.; Reddy, C. D.; Zhang, Y.-W. Effect of Rotational Degrees of Freedom on Molecular Mobility. *J. Phys. Chem. C* **2013**, *117*, 6800–6806.
- (61) Ozmaian, M.; Fathizadeh, A.; Jalalvand, M.; Ejtehadi, M. R.; Allaei, S. M. V. Diffusion and self-assembly of C₆₀ molecules on monolayer graphyne sheets. *Sci. Rep.* **2016**, *6*, 21910.
- (62) Baierlein, R. *Thermal Physics*; Cambridge University Press: Cambridge, U.K., 2003.
- (63) Qian, H.; Sheetz, M. P.; Elson, E. L. Single particle tracking. Analysis of diffusion and flow in two-dimensional systems. *Biophys. J.* **1991**, *60*, 910–921.
- (64) Michalet, X. Mean square displacement analysis of single-particle trajectories with localization error: Brownian motion in an isotropic medium. *Phys. Rev. E* **2010**, *82*, 041914.
- (65) Ernst, D.; Kohler, J. Measuring a diffusion coefficient by single-particle tracking: statistical analysis of experimental mean squared displacement curves. *Phys. Chem. Chem. Phys.* **2013**, *15*, 845–849.
- (66) Arrhenius, S. Über die Reaktionsgeschwindigkeit bei der Inversion von Rohrzucker durch Säuren. *Z. Phys. Chem.* **1889**, *4*, 226–248.